COMPARING IN SITU AND REMOTELY SENSED MEASUREMENTS IN OPTICALLY SHALLOW WATERS

David D. R. Kohler and William D. Philpot,
School of Civil and Environmental Engineering, Cornell University
453 Hollister Hall, Ithaca, NY14853

INTRODUCTION

In situ observations of water-leaving radiance and/or remote sensing reflectance promise to be essential in the development and application of hyperspectral algorithms for coastal passive remotely sensed imagery. To be effective, the link between the in situ and remote measurements must be made very strong. Obviously, the imagery must be accurately georectified and the exact position of the buoy during the image capture must be known to properly link the two. But merely linking the buoy's data to the corresponding pixel in the imagery is usually not sufficient. The heterogeneity of conditions found in coastal environments greatly complicates the relationship between the relatively coarse spatial resolution typical of remote imagery to the small footprint viewed by the buoys. A single coastal image pixel may view several different depths and may include more than one bottom type; this is rarely the case for a typical in situ measurement.

This paper examines several issues that must be addressed in order to relate in situ and remote measurements of water-leaving radiance. Our ultimate goal is to derive water depths from remote hyperspectral imagery. Our imediate task is to relate measurements made using a HyperTSRB (Satlantic, Inc.) to remote measurements. We assume that we will have HyperTSRB measurements (downwelling irradiance, upwelling radiance and depth) in an area where the bottom type and water type are constant and only the depth varies. From these data, we wish to derive enough information about the water and bottom optical properties to be able to extract accurate depths from the remote imagery.

DATA COLLECTION AND DEPTH CORRECTION

The instrument used in this study was the HyperTSRB which gathers downwelling irradiance above the water surface and upwelling radiance (10° half-angle) 66 centimeters below the water surface. In both cases the spectral range is 400-800 nm with a spectral sampling interval of 3.3 nm. Since upwelling radiance at 66 cm can be significantly different than the upwelling radiance at the water surface (particularly in many coastal waters), a correction is required. We attached two radiance detectors to the buoy (Figure 1). Each detector (HOBILabs) was connected via optical fiber to a multi-channel radiometer (Ocean Optics S2000). One detector was mounted at the same depth as the TSRB's radiance collector, the other was placed just below the air-water interface so that it viewed approximately the same area as the first. Using the data from this detector pair, the TSRB's radiance signal can be converted to upwelling radiance above the water surface with the follow equation:

$$L_{uTSRB}(0+) = \left[L_{uTSRB}(0.66-) \frac{L_{uOO}(0-)}{L_{uOO}(0.66-)} \right] t \frac{n_a^2}{n_w^2} \quad (1)$$

where: L_{uTSRB} and L_{uOO} are the radiance values collected using the HyperTSRB and Ocean Optic instruments, respectively; t is the transmittance across the air-water interface; and n_a is the index of refraction for air; and n_w is the index of refraction for water.

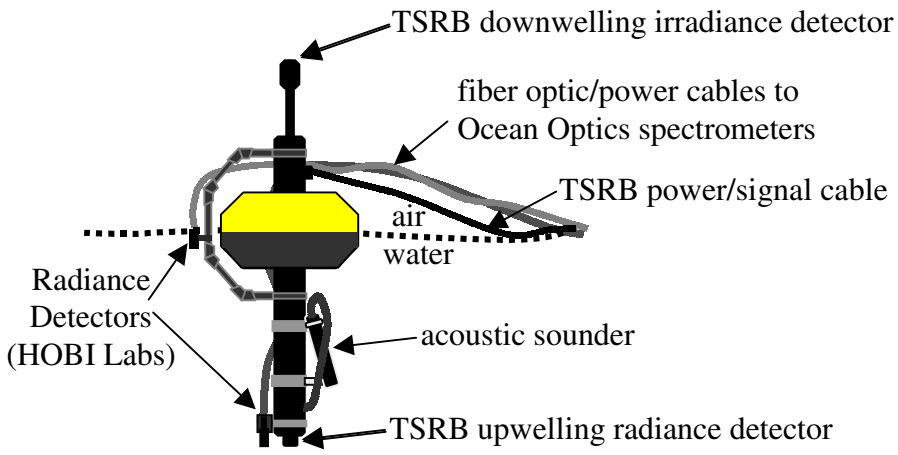

Figure 1: Hyperspectral TSRB (Satlantic, Inc.) fitted with two spectrometers (Ocean Optics S2000) with radiance heads (HOBI Labs) to observe upwelling radiance at 66 cm – coincident with the HTSRB observation – and at 1 cm below the water surface.

MODELING

In deep water it is common to assume that the measurements made by the in situ instrument is representative of the local region in order to relate that measurement to aircraft or satellite data. In shallow waters where the bottom affects the upwelling radiance, this assumption is inadequate. Even if the water properties are locally uniform, there is a good chance that the bottom type and/or depth will vary. In order to develop a connection between in situ and remote data in optically shallow waters, we assume that the water properties and bottom type are locally uniform and that only the water depth is changing. Under these conditions HyperTSRB measurements can be used to derive some coarse characteristics of the water and bottom characteristics. These metrics can then be effectively related to the image data.

Theoretical Background

In one of the first attempts to use passive imagery to derive depth in shallow, coastal waters, researchers at the Environmental Research Institute of Michigan (ERIM) developed a simple model based on reflectance from an optically shallow water column and attenuation of light in a single spectral band (Polcyn and Sattinger, 1969; Polcyn and Lyzenga, 1973, 1979; Lyzenga, 1978, 1979):

$$L_d = L_\infty + L_s e^{-f k z} \tag{2}$$

where: L_d is the radiance received at the airborne detector; L_∞ is a radiance term describing the signal returned from an optically deep water mass; L_s represents the radiance of a wet substrate material (i.e., z = 0); k is the effective attenuation coefficient for the water column; z is the depth of the ocean floor, measuring positively down, starting at zero at the air-water interface; and f is a geometric factor to account for the optical path length through the water. In this notation, taken from Lyzenga (1978), both L_∞ and L_s implicitly include reflectance at the air-sea interface and atmospheric attenuation. Out of necessity, L_∞ also includes path radiance. This model, which states that the upwelling energy from a water body is inversely proportional to its depth, has been the basis of almost all passive imagery investigations of coastal waters to date.

Through the years this model has been refined and improved. Notable improvements include the expansion of the method to include any number of wavebands (Lyzenga, 1978; Philpot, 1989). Also, it was demonstrated that the second term must represent a contrast between the deep water reflectance and the bottom reflectance in order to correctly represent the limits for z = 0 and z = ∞.

We begin with a version of Equation (2) expressed in terms of reflectance (Philpot, 1989):

$$R(0-) = R_\infty + (A_d - R_\infty) e^{-g z} \tag{3}$$

or, rearranging terms:

$$R(0-) = A_d e^{-g z} + (1 - e^{-g z}) R_\infty \tag{4}$$

where: *R(0-)* is the irradiance reflectance just below the water's surface; R_∞ is the irradiance reflectance of an optically deep water column; A_d is the irradiance reflectance of the bottom; g is the effective two-way attenuation coefficient. The variable, g, is a parameter of the single scattering irradiance model (SSI) and should not be confused with k_d, the downwelling diffuse attenuation coefficient integrated over depth (Philpot, 1987). While g is similar to k_d, they are not equal, and are related by:

$$g = k_d + a D_u \tag{5}$$

where: a is the absorption coefficient, and D_u is the distribution function for upwelling irradiance (Preisendorfer, 1976).

If solar illumination, atmospheric effects, and interaction with the air-water interface are included, equation (4) can be expressed in terms of the radiance viewed by the airborne sensor:

$$L_d = C_o T_a (A_d - R_\infty) e^{-g z} + T_a [C_o R_\infty + \rho_a L_k] + L_* \tag{6}$$

where: C_o accounts for the transmission across the air-water interface and the conversion from irradiance to radiance; T_a is the atmospheric transmission factor; ρ_a is the Fresnel reflectance in the air; L_k is the sky radiance, and L_* is the atmospheric path radiance. Equation (6) will be more manageable if some terms are combined. Two new terms are introduced to accomplish this:

$$L_b = C_o T_a (A_d - R_\infty) \tag{7}$$

$$L_\infty = T_a [C_o R_\infty + \rho_a L_k] + L_* \tag{8}$$

Clearly, L_b represents the contrast between the bottom and water reflectance, while L_∞ is dependent on atmospheric effects, the surface reflectance, and the reflectance from optically deep water (Philpot, 1989). We may now write an expression for the remotely sensed radiance in terms of the deep water radiance and a depth-dependent radiance term:

$$L_d = L_\infty + L_b e^{-g z} \tag{9}$$

Equation (9) is identical in form to Equation (2), but it is Equation (9), with its components as defined above, that will serve as our basic model for this study.

Calibrating the model

Equation (9) can easily be solved for depth, z, if the other variables are known. L_d is measured directly by the remote system, and L_∞ is often taken from a nearby, deep water measurement. But, L_b and g are still unknowns but can be found using the corrected, *in situ* measurements made with the HyperTSRB. The buoy's data set must cover several depths while the bottom and water type remained unvaried. The depth at these points was provided by an acoustic sounder mounted on the HyperTSRB (Figure 1). Rearranging equation (9):

$$\ln\left(L_d - L_\infty\right) = \ln\left(L_b\right) - g z \tag{10}$$

we may solve for L_b and g using linear regression.

Unfortunately, gathering a data set that is sufficiently complete to perform the above analysis is difficult and rare. For example, it may be possible to find an area of constant water and bottom type where the depth varies. But it is often difficult to find a deep water signal, L_∞, close enough to assume that it water properties are the same as in the shallow area. It is more likely to find an area with the same bottom type but only a limited range of depths. In that case it is still possible to solve for L_b and g using optimization procedures. To do this, equation (10) was first solved by temporarily equating L_∞ with the deepest measured corrected upwelling signal. This produced initial estimates for L_b and g. Next, by altering L_∞ the following equation was optimized.

$$\sigma^2 \left[\frac{L_d - L_\infty}{\exp(-g z_i)} \right] = 0 \tag{11}$$

where: σ^2 represents the variance of the sample. This was done for every wavelength in the sample. Finally, the L_∞ spectra that best fit equation (11) was inserted back into the first step to find an improved estimate for L_b and g. This procedure was iterated until all of the L_b, L_∞, and g spectra converged.

DATA SET DEVELOPMENT

In order to test the validity of the above optimization, a synthetic data set was developed using HYDROLIGHT 4.0. This program solves the radiative transfer equation (RTE) through numerical methods (Mobley, 1998) given the optical properties of the water column and the bottom.

The HYDROLIGHT runs were made using default data provided with the program. These data cover the range of expected conditions found in the field. The spectral output was chosen to span from 350 to 700 nanometers with a bandwidth of 10 nanometers. Only the coral sand bottom types were used. The depths of interest selected were: 2.0m, 3.0m, 4.0m, 5.0m, 6.0m, 7.0m, 8.0m, 9.0m, 10.0m, 13.0m, 16.0m and infinitely deep water (50 meters). These depths were chosen because each depth produced a signal that was spectrally different from both optically deep water and one another. A HYDROLIGHT run was performed to generate spectra of the remotely sensed radiance, L_d, for each of these depths. In practice, L_d would be derived directly from HyperTSRB measurements made at different water depths over one bottom type.

RESULTS AND DISCUSSION

In order to test how the optimization would perform with limited data sets, the algorithm was run using data with different depth ranges. The first run used data for the 2.0-6.0 meter range. On each subsequent run the next deeper depth was added.

Figure 2 and Figure 3 show the L_b and g spectra, respectively, derived for each of the runs. These graphs clearly show that, regardless of the limited depth range of the input data, the shape and magnitude of the optimized spectra are very similar. Figure 4 shows the predictions for L_∞ given the values for L_b and g for a each data set. While all the spectra have approximately the same magnitude, spectra based on the two most limited data sets have noticeably different shapes, probably because we are extrapolating too far from the original data set.

Finally, since the ultimate point of this process is to produce estimates of water depth, the optimized values for the L_b, L_∞, and g spectra were used to predict the water depth and compared to the true depth (i.e., the modeled water depth). This was done using the procedure suggested by Philpot (1989) using Principal Components Analysis (PCA) produce more accurate depth estimates using spectral data. However, before PCA could be used, some preprocessing of the data was necessary. Because attenuation is higher at some wavelengths than at others, the "shallow water" signal (L_d) can be distinct from the optically deep water at some wavelength while it is indistinguishable from deep water at other wavelengths. At wavelengths for which L_d is indistinguishable from L_∞ the log of the difference between the detected value and the infinitely deep water, $L_d - L_\infty$, is undefined and would cause the PCA procedure to fail even though a solution would be possible at other wavelengths. To avoid this error only upwelling signals from water depths of less than 10 meters were used in this part of the analysis.

Because the PCA was performed on data for which depth was the only variable, the first principal component explained over 95% of the variance in the synthetic data set.

With the principal components calculated, the next step was to retrieve the depths. The derived first principal component vector, a_{PC1}, was multiplied by equation (9) to produce:

$$z = \frac{-\left[a_{PC1} \bullet \ln\left|L_d - L_\infty\right| - a_{PC1} \bullet \ln\left|L_b\right|\right]}{a_{PC1} \bullet g} \qquad (12)$$

This vector product weights each wavelength so as to generate a more accurate overall depth estimate than could be obtained from any single wavelength.

A graph of the accuracy of the predictions generated from each of the incomplete data sets is shown in figure 4. The predictions are very good for depths within the range of the observations. The relatively poor results that 2 to 6 meter data set and the 2 to 7 meter data set are due primarily to the less than optimal L_∞ spectra each generated.

SUMMARY

In this paper we have outlined a procedure to derive water depths from remote hyperspectral imagery based on parameters derived from a set of in situ hyperspectral observations. The procedure begins with a correction of the HyperTSRB measurements for the depth of the upwelling radiance sensor. The corrected values for L_d can then be used to derive spectral parameters, L_b, L_∞, and g, which are the basis for optimizing the depth estimate.

This research was supported by the Office of Naval Research, Environmental Optics Program, under contract N00014-97-1-0721.

REFERENCES

Lyzenga, D. R. (1978*). Passive Remote Sensing Techniques for Mapping Water depth and Bottom Features*. Applied Optics, 17 (3) . pp 378-383.

Lyzenga, D. R. (1979*). Shallow Water Reflectance Modeling with Applications to Remote Sensing*. Proceedings of 13th International Symposium on Remote Sening of Environment. pp. 583-602.

Mobley, C. D. (1998*).* Hydrolight 3.0 Users' Guide. Sequoia Scientific, Inc.: Mercer Island, WA.

Mobley, C. D. (1994). Light and Water: Radiative Transfer in Natural Waters. Academic Press: New York

Philpot, W. D. (1987*). Radiative Transfer in Stratified Waters: A Single-Scattering Approximation for Irradiance*. Applied Optics, 26 (19). pp 4123-4132.

Philpot, W. D. (1989*). Bathymetry Mapping with Passive Multispectral Imagery*. Applied Optics, 28 (8). pp 1569-1578.

Polcyn, F. C., and Lyzenga, D. R. (1973*). Calculations of Water Depth from ERTS-MSS Data*. Symposium of Significant Results from ERTS-1. NASA Spec, Publ. SP-327. pp. 1433-1436.

Polcyn, F. C., and Lyzenga, D. R. (1979*). Landsat Bathymetry Mapping by Multitemproral Processing*. Proceedings of 13th International Symposium on Remote Sening of Environment. pp. 1269-1276.

Polcyn, F. C., and Sattinger, I. J. (1969*). Water Depth Determination Using Remote Sensing Techniques*. Proceedings of the 6th International Symposium on Remote Sensing of Environment. pp 1017-1028.

Preisendorfer, R.W. (1976) Hydrologic Optics, Vol 5, pg. 10. U.S. Department of Commerce USGPO, 1976-678-487/56 Region 8.

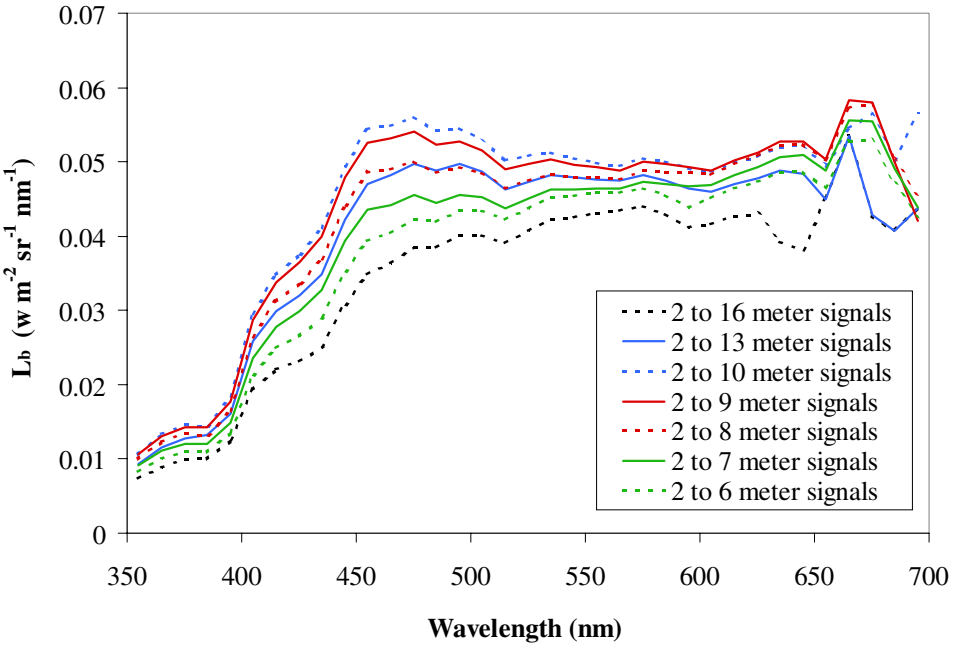

Figure 2: Estimates for L_b using incomplete data sets.

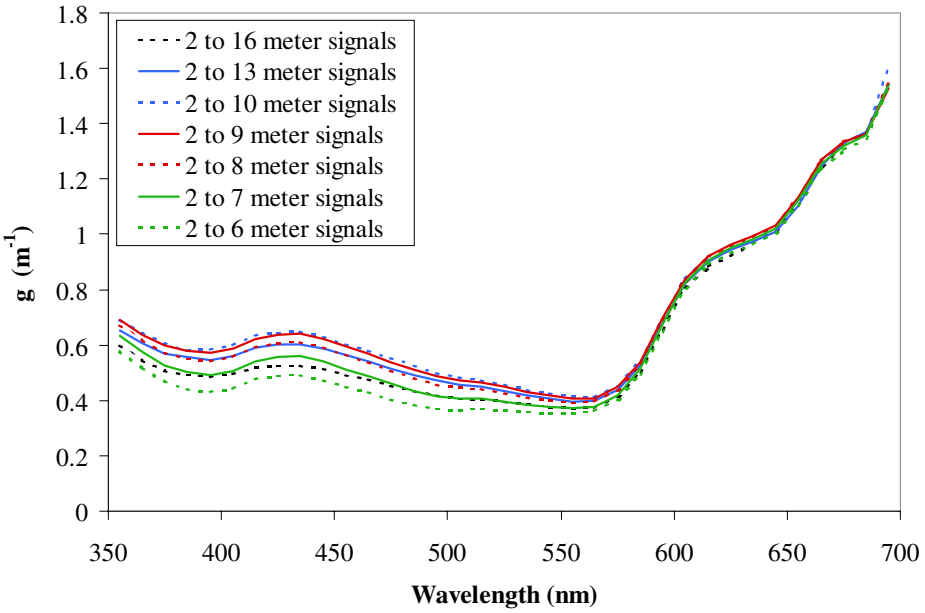

Figure 3: Estimates for the effective attenuation coefficient, g, using incomplete data sets

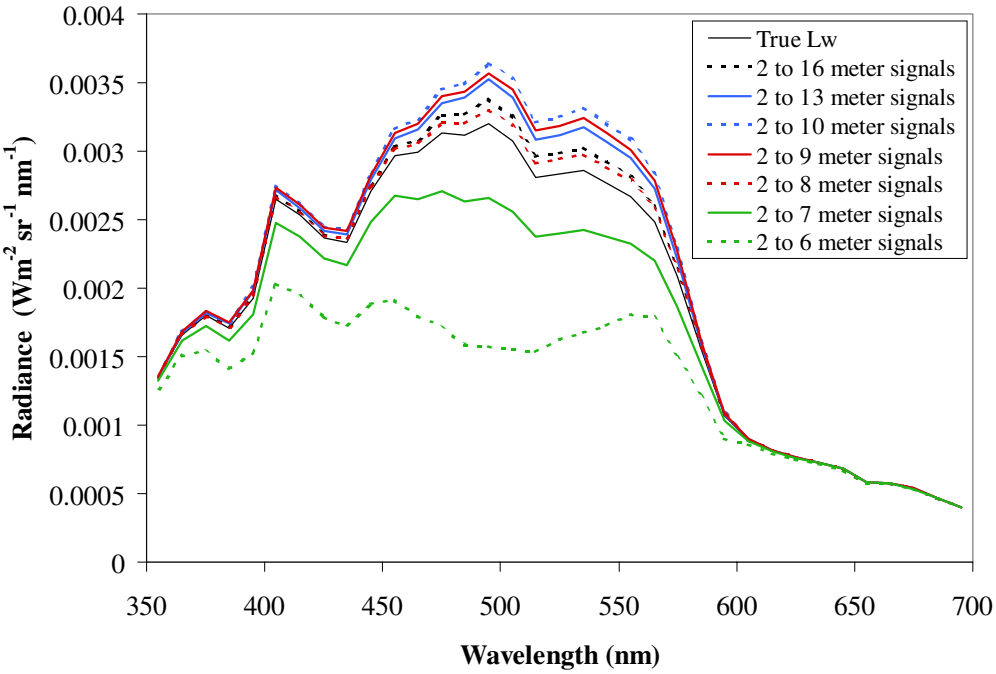

Figure 4: Radiance for optically deep water, L_{∞}, estimated using incomplete data sets

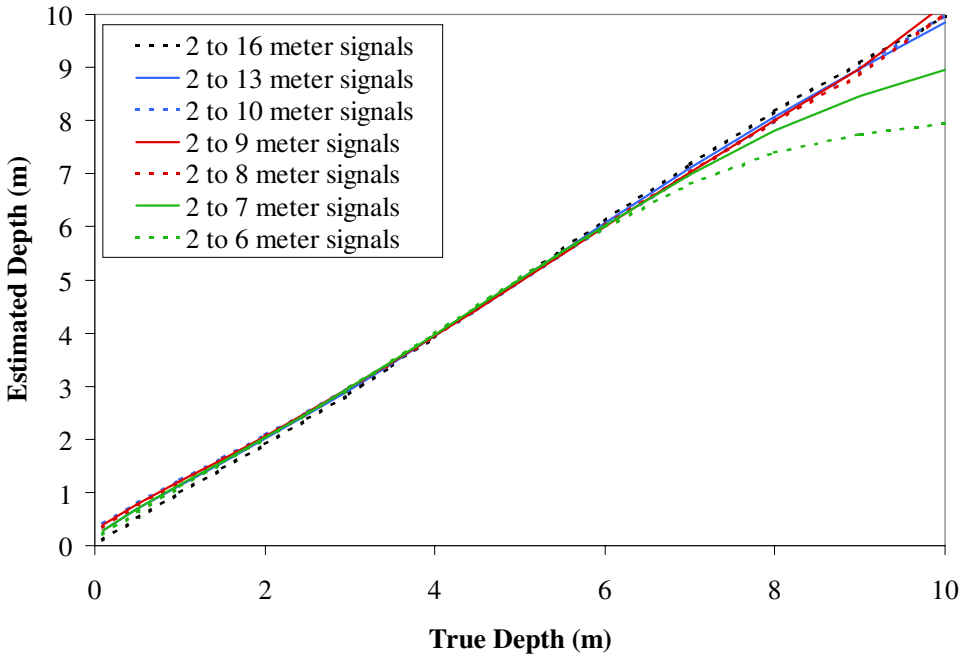

Figure 5: Depth estimation using incomplete data sets